AIAA JOURNAL
Vol. 39, No. 10, October 2001

Development of Isoparametric, Degenerate Constrained Layer Element for Plate and Shell Structures

Y. S. Jeung*
Korea Aerospace Industries, Seoul 120-709, Republic of Korea
and
I. Y. Shen†
University of Washington, Seattle, Washington 98195-2600

An isoparametric, degenerate element for constrained layer damping treatments is presented. The element is valid for either plate or shell structures. The element is an 18-node degenerate element with nine nodes located on the base shell (or plate) structure and nine nodes on the constraining layer. Each node has five degrees of freedom: translations in x, y, and z and bending rotations α and β about the midsurface where the node is located. The displacement field of the viscoelastic layer is interpolated linearly from the nodal displacements; therefore, the viscoelastic layer allows both shear and normal deformations. The base shell (or plate) structure and the constraining layer can be linearly elastic or piezoelectric for passive or active applications. The viscoelastic layer is assumed to be linearly viscoelastic. The equation of motion is derived through use of the principle of virtual work. For thin plate structures, numerical results show that the isoparametric element can predict natural frequencies, loss factors, and mechanical impedances that are as accurate as NASTRAN with substantially fewer elements. For thin shell structures, locking and spurious modes need to be resolved to yield reasonable results.

I. Introduction

CONSTRAINED layer treatments have been used for years to reduce structural and machine vibration.[1,2] For simple one-dimensional structural components, for example, beams, closed-form solutions are still possible. For two-dimensional structural components, such as plates and shells, it is more practical to obtain meaningful solutions through finite element calculations. In the past, researchers have developed various finite element formulations for constrained layer structures. Basically, there are two different approaches.

The first approach is to use existing finite element codes, such as NASTRAN, to analyze constrained layer plates and shells. For example, Lu et al.[3] analyzed constrained layer plates with NASTRAN. The plates and the constraining layers were modeled by plate elements, and the viscoelastic layers were modeled by brick elements. Soni and Bogner[4] used MAGNA to analyze constrained layer treatments. The constraining layers and the base structures were modeled by eight-node thin shell elements or penalty function shell elements. The viscoelastic layer was modeled by eight-node solid elements with reduce integration. Johnson and Kienholz[5] applied NASTRAN to analyze vibration of beams, rings, and plates with constrained layer damping. For constrained layer plates, they modeled the constraining layers and the base structures through plate elements and modeled the viscoelastic cores with solid elements. Lu and Killian[6] analyzed damped plate composites by using NASTRAN. The constraining layers and the base strctures were modeled with homogeneous four-node quadrilateral plate elements. The viscoelastic cores were modeled with linear isoparametric eight-node brick elements. Numerical results were obtained in the form of driving point mechanical impedance. Imaino and Harrison[7] used the P-code, which uses higher-order base function and can model systems with high aspect ratios with relatively few elements, developed at IBM, to analyze vibration of partially treated beam. Macé[8] used NASTRAN to verify a new theory developed for constrained layer beams.

The second approach is to develop new elements for structural components with constrained layer treatments. These new elements can vary substantially because different elements have different assumptions. For example, Ioannides and Grootenhuis[9] developed a triangular plate element. They assumed that all three layers had the same deflection and slopes. Therefore, the plate element had two in-plane displacements for the constraining layer, two in-plane displacements for the base plate, and one out-of-plane deflection and two slopes for all three layers. They also performed experiments on circular plates and beams with different boundary conditions. Rikards et al.[10] developed a six-node triangular plate element. Three nodes were on the constraining layer and three on the base plate. The displacement field of the viscoelastic layer was determined through kinematic compatibility, that is, no-slip conditions. Each node had six degrees of freedom: that is, three translational and three rotational. They performed numerical tests on rectangular plates. Rao et al.[11] developed offset beam elements and shear deformation viscoelastic elements to model constrained layer damping. Ramesh and Ganesan[12,13] analyzed vibration and damping of cylindrical shells with a viscoelastic core. They used two-node finite elements based on different shell theories. References 14–17 list other research work along this line.

The purpose of this paper is to develop an 18-node isoparametric element for plate or shell structures with constrained layer treatments. Compared with the constrained layer elements reported in Refs. 9–17, the uniqueness of this new element is twofold. First, it is an isoparametric constrained layer element. Therefore, the formulation uses natural coordinates making it possible to generate elements that are nonrectangular with curved sides. Second, this constrained layer element is not limited to a specific shell geometry, such as cylindrical shells.[12,13] This is in line with a comment made by Bathe and Dvorkin[18] that finite element methods for shell structures should be formulated without use of a specific shell theory so that the methods are applicable to any plates and shells.

To achieve these goals, this paper adopts the degenerate shell element by Ahmad et al.[19] for the constraining layer and the base shell structure. Basically, this element follows Mindlin theory and assumes plane stress condition. There are nine nodes on each of the constraining layers and the base shell structure. The displacement field of the viscoelastic layer is linearly interpolated through no-slip boundary conditions at the layer interfaces.

The nine-node formulation is selected because of several considerations. First, all isoparametric elements lose accuracy when distorted from the rectangular shape. However, the nine-node Lagrange element is less sensitive than the eight-node serendipity element to

Received 30 November 1999; revision received 28 October 2000; accepted for publication 6 April 2001.

*Senior Manager and Chief, Fixed Wing Programs II.
†Associate Professor, Department of Mechanical Engineering.

nonrectangularity, curvatures of sides, and placing side nodes away from midsides. Second, most lumping schemes for generating mass matrices result in positive nodal masses for nine-node elements, but may lead to negative nodal masses for eight-node elements.[20] Third, nine-node shell elements can pass constant-curvature patch tests with bilinear element geometry, but eight-node shell elements cannot.[21] In general, the ninth interior node of the Lagrange element acquires real significance in dynamics problems.

This paper first discusses the isoparametric formulation of the constrained layer element including geometric definition of the element, shape functions, displacement fields, the Jacobian matrix, coordinate transformation, the strain-displacement matrix, and the stress-strain matrix. Use of the principle of virtual work leads to the element stiffness matrix, nodal load vectors, and the element mass matrix. Solution of the equation of motion can result in eigenvalues, that is, damped natural frequencies and loss factors, and frequency-response functions. Finally, numerical results are compared with those from the literature.

II. Formulation

Figure 1 shows the geometry and coordinate systems of the isoparametric element developed in this paper. Layers 1 and 3 are linear piezoelectric, and layer 2 is linear viscoelastic. This element will be valid for a passive constrained layer treatment if both layers 1 and 3 are elastic. This element will be valid for an active constrained layer shell treatment, if either layer 1 or layer 3 is elastic. This element will reduce to a traditional isoparametric shell element if layer 1 is elastic and layers 2 and 3 are absent. In the following, quantities related to the jth layer is denoted by a superscript (j), and quantities related to the ith node is denoted by a subscript i. Sometimes, subscript j will also denote quantities related to the jth layer, should there be no confusion. For example, t_i denotes the thickness of the ith layer. Finally, the isoparametric element assumes the following two kinematic conditions. First, all three layers are perfectly bonded. Second, layers 1 and 3 follow Mindlin plate theory.

There are three coordinate systems associated with the element. The first coordinate system is the global coordinate system x, y, and z, which is fixed in the space (Fig. 1). The second coordinate system is the local coordinate system x', y', and z' defined at each node. The z' axis is in the thickness direction. The x' and y' axes are tangent to the midsurface of the shell and define the axes of nodal rotation (Fig. 1). The third set of coordinate systems, is the natural coordinates ξ, η, and ζ (see Fig. 2). Moreover, all three layers share the same ξ and η coordinates, but each layer has its own $\zeta^{(i)}$ coordinates, such as $\zeta^{(1)}$, $\zeta^{(2)}$, and $\zeta^{(3)}$. Therefore, the natural coordinates ξ, η, and $\zeta^{(i)}$ define the ith layer of the element through $\xi = \pm 1$, $\eta = \pm 1$, and $\zeta^{(i)} = \pm 1$. Transformation among these three coordinate systems will be explained in detail after the shape functions are introduced.

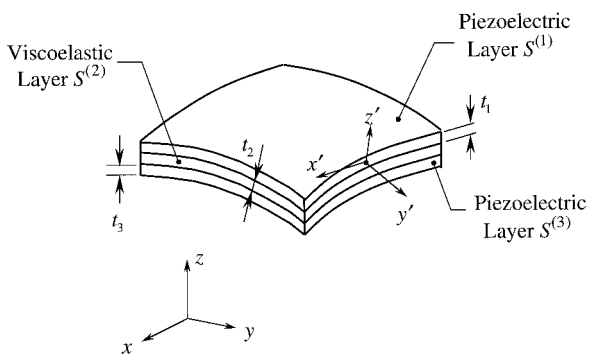

Fig. 1 Geometry and coordinate systems of the isoparametric element.

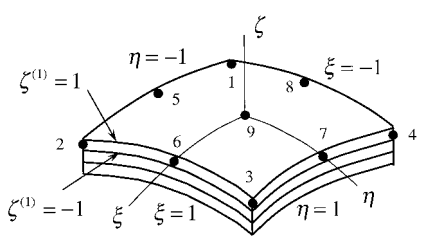

Fig. 2 Natural coordinates and nodes of layer 1 of the element.

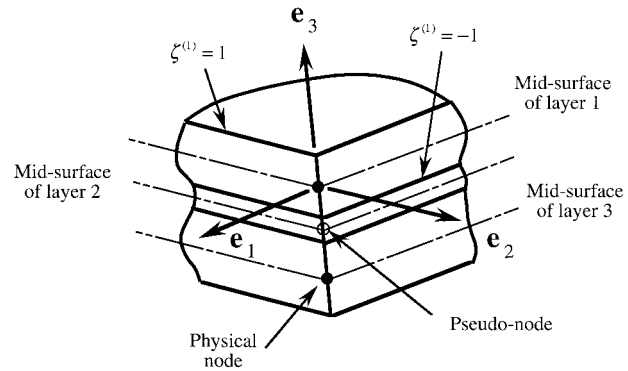

Fig. 3 Physical and pseueonodes of the element.

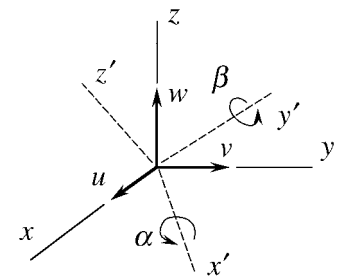

Fig. 4 Translational and rotational nodal degrees of freedom.

The element is an 18-node degenerate shell element. There are nine physical nodes on layers 1 (Fig. 2) and nine physical nodes on layer 3. The nodes are located on the midsurface of each layer (Fig. 3). In addition, there are nine pseudonodes located on the viscoelastic layer 2. The purpose of the pseudonodes is to simplify the derivation. They will not appear as independent degrees of freedom.

Each node has three translational degrees of freedom u, v, and w in the global coordinates and two rotational degrees of freedom α and β about the local coordinates (Fig. 4). Note that the rotation about the z' axis is not considered because of the assumptions made in the Mindlin theory.

A. Shape Functions

In isoparametric formulations, shape functions are used to interpolate the position and the displacement fields simultaneously within the element through the natural coordinates. For the nodes in Fig. 2, the vector of shape functions $\boldsymbol{N}$ is given by

$$\boldsymbol{N} = \boldsymbol{X}\Psi \tag{1}$$

where

$$\boldsymbol{N} \equiv [N_1, N_2, \ldots, N_9] \tag{2}$$

$$\boldsymbol{X} \equiv [1, \xi, \eta, \xi^2, \xi\eta, \eta^2, \xi^2\eta, \xi\eta^2, \xi^2\eta^2] \tag{3}$$

$$\Psi = \frac{1}{4}\begin{bmatrix} 0 & 0 & 0 & 0 & 0 & 0 & 0 & 0 & 4 \\ 0 & 0 & 0 & 0 & 0 & 2 & 0 & -2 & 0 \\ 0 & 0 & 0 & 0 & -2 & 0 & 2 & 0 & 0 \\ 0 & 0 & 0 & 0 & 0 & 2 & 0 & 2 & -4 \\ 1 & -1 & 1 & -1 & 0 & 0 & 0 & 0 & 0 \\ 0 & 0 & 0 & 0 & 2 & 0 & 2 & 0 & -4 \\ -1 & -1 & 1 & 1 & 2 & 0 & -2 & 0 & 0 \\ -1 & 1 & 1 & -1 & 0 & -2 & 0 & 2 & 0 \\ 1 & 1 & 1 & 1 & -2 & -2 & -2 & -2 & 4 \end{bmatrix} \tag{4}$$

Note that the shape function $N_i(\xi, \eta)$ is 1 at node i and zero at other nodes.

B. Definition of Local Coordinates

First, let us consider the midsurface of the jth layer ($\zeta^{(j)}=0$). The position of any point on the midsurface can be interpolated in terms of the nine nodal positions through

$$\begin{Bmatrix} x \\ y \\ z \end{Bmatrix}^{(j)}_{\zeta^{(j)}=0} = \sum_{i=1}^{9} N_i(\xi,\eta) \begin{Bmatrix} x_i \\ y_i \\ z_i \end{Bmatrix}^{(j)}, \qquad j=1,2,3 \quad (5)$$

Equation (5) can be used to define the local coordinates x', y', and z' as follows. Let $\boldsymbol{v}_1$ and $\boldsymbol{v}_2$ be vectors tagent to x' and y'. Therefore,

$$\boldsymbol{v}_1 \equiv \frac{\partial}{\partial\xi} \begin{Bmatrix} x \\ y \\ z \end{Bmatrix}^{(j)}_{\zeta^{(j)}=0} = \sum_{i=1}^{9} N_{i,\xi}(\xi,\eta) \begin{Bmatrix} x_i \\ y_i \\ z_i \end{Bmatrix}^{(j)} \quad (6)$$

where $N_{i,\xi}$ means the partial derivative of $N_i(\xi,\eta)$ with respect to ξ. Similarly,

$$\boldsymbol{v}_2 \equiv \frac{\partial}{\partial\eta} \begin{Bmatrix} x \\ y \\ z \end{Bmatrix}^{(j)}_{\zeta^{(j)}=0} = \sum_{i=1}^{9} N_{i,\eta}(\xi,\eta) \begin{Bmatrix} x_i \\ y_i \\ z_i \end{Bmatrix}^{(j)} \quad (7)$$

Finally, the unit vectors $\boldsymbol{e}_1$, $\boldsymbol{e}_2$, and $\boldsymbol{e}_3$ along the local coordinates are

$$\boldsymbol{e}_1 = \boldsymbol{v}_1/|\boldsymbol{v}_1|, \qquad \boldsymbol{e}_2 = \boldsymbol{v}_2/|\boldsymbol{v}_2|, \qquad \boldsymbol{e}_3 = \boldsymbol{e}_1 \times \boldsymbol{e}_2 \quad (8)$$

Because $\boldsymbol{e}_1$, $\boldsymbol{e}_2$, and $\boldsymbol{e}_3$ are unit vectors, their vector components are directional cosines denoted as

$$\boldsymbol{e}_1 = \begin{Bmatrix} l_1 \\ m_1 \\ n_1 \end{Bmatrix}, \qquad \boldsymbol{e}_2 = \begin{Bmatrix} l_2 \\ m_2 \\ n_2 \end{Bmatrix}, \qquad \boldsymbol{e}_3 = \begin{Bmatrix} l_3 \\ m_3 \\ n_3 \end{Bmatrix} \quad (9)$$

C. Geometric Definition of the Element

Now consider the position of any point inside the jth layer. The position vector consists of a midsurface component [cf. Eq. (5)] and a thickness component related to $\boldsymbol{e}_3$, that is,

$$\begin{Bmatrix} x \\ y \\ z \end{Bmatrix}^{(j)} = \sum_{i=1}^{9} N_i(\xi,\eta) \begin{Bmatrix} x_i \\ y_i \\ z_i \end{Bmatrix}^{(j)} + \frac{t_j\zeta^{(j)}}{2} \sum_{i=1}^{9} N_i(\xi,\eta)\boldsymbol{e}_{3i}^{(j)}$$

$$j=1,2,3 \quad (10)$$

Because the viscoelastic layer has pseudonodes, they are not independent and need to be represented in terms of the other nodes on layers 1 and 3. Note that the global coordinates obtained from two adjacent layers at the layer interfaces must be identical; therefore,

$$\begin{Bmatrix} x \\ y \\ z \end{Bmatrix}^{(1)}_{\zeta^{(1)}=-1} = \begin{Bmatrix} x \\ y \\ z \end{Bmatrix}^{(2)}_{\zeta^{(2)}=1}, \qquad \begin{Bmatrix} x \\ y \\ z \end{Bmatrix}^{(2)}_{\zeta^{(2)}=-1} = \begin{Bmatrix} x \\ y \\ z \end{Bmatrix}^{(3)}_{\zeta^{(3)}=1} \quad (11)$$

Substitution of Eq. (11) into Eq. (10) leads to

$$\sum_{i=1}^{9} N_i(\xi,\eta) \begin{Bmatrix} x_i \\ y_i \\ z_i \end{Bmatrix}^{(2)} = \frac{1}{2} \left(\begin{Bmatrix} x \\ y \\ z \end{Bmatrix}^{(1)}_{\zeta^{(1)}=-1} + \begin{Bmatrix} x \\ y \\ z \end{Bmatrix}^{(3)}_{\zeta^{(3)}=1} \right) \quad (12)$$

$$\frac{t_2}{2} \sum_{i=1}^{9} N_i(\xi,\eta)\boldsymbol{e}_{3i}^{(2)} = \frac{1}{2} \left(\begin{Bmatrix} x \\ y \\ z \end{Bmatrix}^{(1)}_{\zeta^{(1)}=-1} - \begin{Bmatrix} x \\ y \\ z \end{Bmatrix}^{(3)}_{\zeta^{(3)}=1} \right) \quad (13)$$

Substitution of Eqs. (12) and (13) back to Eq. (10) results in

$$\begin{Bmatrix} x \\ y \\ z \end{Bmatrix}^{(2)} = \frac{1}{2}\left(1+\zeta^{(2)}\right) \begin{Bmatrix} x \\ y \\ z \end{Bmatrix}^{(1)}_{\zeta^{(1)}=-1} + \frac{1}{2}\left(1-\zeta^{(2)}\right) \begin{Bmatrix} x \\ y \\ z \end{Bmatrix}^{(3)}_{\zeta^{(3)}=1} \quad (14)$$

where the positions of layers 1 and 3 can be found through Eq. (10).

D. Displacement Field

Consider a point P with natural coordinates $(\xi,\eta,\zeta^{(j)})$ inside layer 1 or layer 3. The projection of P on its midsurface is P' and has natural coordinates $(\xi,\eta,0)$. The displacement of P consists of two parts: translation of P' and the rotation of P about P'. Therefore, the displacement field in layers 1 and 3 can be represented as

$$\begin{Bmatrix} u \\ v \\ w \end{Bmatrix}^{(j)} = \begin{Bmatrix} u \\ v \\ w \end{Bmatrix}^{(j)}_{\zeta^{(j)}=0} + \frac{t_j\zeta^{(j)}}{2}\left[\alpha\boldsymbol{e}_1^{(j)} \times \boldsymbol{e}_3^{(j)} + \beta\boldsymbol{e}_2^{(j)} \times \boldsymbol{e}_3^{(j)}\right] \quad (15)$$

In addition, the translational displacements u, v, and w and angular displacements α and β can be interpolated through shape functions in terms of nodal displacements as

$$\begin{Bmatrix} u \\ v \\ w \end{Bmatrix}^{(j)} = \sum_{i=1}^{9} N_i(\xi,\eta) \begin{Bmatrix} u_i \\ v_i \\ w_i \end{Bmatrix}^{(j)} + \frac{t_j\zeta^{(j)}}{2} \sum_{i=1}^{9} N_i(\xi,\eta)\Theta_i^{(j)} \begin{Bmatrix} \alpha_i \\ \beta_i \end{Bmatrix}^{(j)}$$

$$j=1,3 \quad (16)$$

where

$$\Theta_i^{(j)} = \left[-\boldsymbol{e}_{2i}^{(j)}, \boldsymbol{e}_{1i}^{(j)}\right] = \begin{bmatrix} -l_{2i}^{(j)} & l_{1i}^{(j)} \\ -m_{2i}^{(j)} & m_{1i}^{(j)} \\ -n_{2i}^{(j)} & n_{1i}^{(j)} \end{bmatrix} \quad (17)$$

Finally, Eq. (16) can be rearranged into a matrix form

$$\begin{Bmatrix} u \\ v \\ w \end{Bmatrix}^{(j)} = \sum_{i=1}^{9} \boldsymbol{N}_i^{(j)} \begin{Bmatrix} u_i \\ v_i \\ w_i \\ \alpha_i \\ \beta_i \end{Bmatrix}^{(j)}, \qquad j=1,3 \quad (18)$$

where

$$\boldsymbol{N}_i^{(j)} = N_i(\xi,\eta) \left[\begin{bmatrix} 1 & 0 & 0 \\ 0 & 1 & 0 \\ 0 & 0 & 1 \end{bmatrix}, \frac{t_j\zeta^{(j)}}{2}\Theta_i^{(j)} \right] \quad (19)$$

For layer 2, the displacement field is interpolated linearly in $\zeta^{(2)}$ resulting in

$$\begin{Bmatrix} u \\ v \\ w \end{Bmatrix}^{(2)} = \frac{1+\zeta^{(2)}}{2} \begin{Bmatrix} u \\ v \\ w \end{Bmatrix}^{(2)}_{\zeta^{(2)}=1} + \frac{1-\zeta^{(2)}}{2} \begin{Bmatrix} u \\ v \\ w \end{Bmatrix}^{(2)}_{\zeta^{(2)}=-1} \quad (20)$$

As a result of the no-slip condition at the layer interfaces, Eq. (20) can be rewritten as

$$\begin{Bmatrix} u \\ v \\ w \end{Bmatrix}^{(2)} = \frac{1+\zeta^{(2)}}{2} \begin{Bmatrix} u \\ v \\ w \end{Bmatrix}^{(1)}_{\zeta^{(1)}=-1} + \frac{1-\zeta^{(2)}}{2} \begin{Bmatrix} u \\ v \\ w \end{Bmatrix}^{(3)}_{\zeta^{(3)}=1} \quad (21)$$

Substitution of Eq. (18) into Eq. (21) results in the displacement field of layer 2 in terms of nodal displacements of layers 1 and 3 as

$$\begin{Bmatrix} u \\ v \\ w \end{Bmatrix}^{(2)} = \sum_{i=1}^{9} \boldsymbol{Q}_i^{(1)} \begin{Bmatrix} u_i \\ v_i \\ w_i \\ \alpha_i \\ \beta_i \end{Bmatrix}^{(1)} + \sum_{i=1}^{9} \boldsymbol{Q}_i^{(3)} \begin{Bmatrix} u_i \\ v_i \\ w_i \\ \alpha_i \\ \beta_i \end{Bmatrix}^{(3)} \quad (22)$$

where

$$\boldsymbol{Q}_i^{(1)} \equiv \frac{1+\zeta^{(2)}}{2}\boldsymbol{N}_i^{(1)}\bigg|_{\zeta^{(1)}=-1}, \qquad \boldsymbol{Q}_i^{(3)} \equiv \frac{1-\zeta^{(2)}}{2}\boldsymbol{N}_i^{(3)}\bigg|_{\zeta^{(3)}=1} \tag{23}$$

The displacement relations (18) and (22) can be written in a more compact form within an element. For the ith node, define the 5×1 nodal displacement vector $\boldsymbol{d}_i^{(j)}$ as

$$\boldsymbol{d}_i^{(j)} = \{u_i, v_i, w_i, \alpha_i, \beta_i\}^{(j)} \tag{24}$$

For each element, there are nine nodes in layer 1 and nine nodes in layer 3. Therefore, each element has 90 degrees of freedom defining a nodal displacement vector $\boldsymbol{d}$ through

$$\boldsymbol{d} = \left\{\boldsymbol{d}_1^{(1)}, \boldsymbol{d}_2^{(1)}, \ldots, \boldsymbol{d}_9^{(1)}, \boldsymbol{d}_1^{(3)}, \boldsymbol{d}_2^{(3)}, \ldots, \boldsymbol{d}_9^{(3)}\right\}^T \tag{25}$$

Finally, the displacement field $\boldsymbol{u}^{(j)}$ of the jth layer can be interpolated by the nodal displacement vector $\boldsymbol{d}$ through

$$\boldsymbol{u}^{(j)}\left(\xi, \eta, \zeta^{(j)}\right) \equiv \begin{Bmatrix} u \\ v \\ w \end{Bmatrix}^{(j)} = \boldsymbol{N}^{(j)}\left(\xi, \eta, \zeta^{(j)}\right)\boldsymbol{d}, \qquad j = 1, 2, 3 \tag{26}$$

where $\boldsymbol{N}^{(j)}(\xi, \eta, \zeta^{(j)})$ is the matrix of shape functions for the jth layer. For layers 1 and 3, comparison of Eqs. (18) and (26) results in

$$\boldsymbol{N}^{(1)} = \left[\boldsymbol{N}_1^{(1)}, \boldsymbol{N}_2^{(1)}, \ldots, \boldsymbol{N}_9^{(1)}, \boldsymbol{0}, \boldsymbol{0}, \ldots, \boldsymbol{0}\right] \tag{27}$$

$$\boldsymbol{N}^{(3)} = \left[\boldsymbol{0}, \boldsymbol{0}, \ldots, \boldsymbol{0}, \boldsymbol{N}_1^{(3)}, \boldsymbol{N}_2^{(3)}, \ldots, \boldsymbol{N}_9^{(3)}\right] \tag{28}$$

For layer 2, comparison of Eqs. (22) and (26) results in

$$\boldsymbol{N}^{(2)} = \left[\boldsymbol{Q}_1^{(1)}, \boldsymbol{Q}_2^{(1)}, \ldots, \boldsymbol{Q}_9^{(1)}, \boldsymbol{Q}_1^{(3)}, \boldsymbol{Q}_2^{(3)}, \ldots, \boldsymbol{Q}_9^{(3)}\right] \tag{29}$$

E. Jacobian Matrix

The Jacobian matrix $\boldsymbol{J}$ is needed to formulate integrals in the natural coordinates. Let $\boldsymbol{J}$ be

$$\boldsymbol{J} = \begin{bmatrix} x_{,\xi} & y_{,\xi} & z_{,\xi} \\ x_{,\eta} & y_{,\eta} & z_{,\eta} \\ x_{,\zeta} & y_{,\zeta} & z_{,\zeta} \end{bmatrix} \tag{30}$$

Then the differential element $\mathrm{d}x\,\mathrm{d}y\,\mathrm{d}z$ in the global coordinates can be represented in terms of $\mathrm{d}\xi\,\mathrm{d}\eta\,\mathrm{d}\zeta$ in the natural coordinates through

$$\mathrm{d}x\,\mathrm{d}y\,\mathrm{d}z = |\boldsymbol{J}|\,\mathrm{d}\xi\,\mathrm{d}\eta\,\mathrm{d}\zeta \tag{31}$$

To determine $\boldsymbol{J}$, substitution of Eq. (10) into Eq. (30) results in

$$\frac{\partial}{\partial\xi}\begin{Bmatrix} x \\ y \\ z \end{Bmatrix}^{(j)} = \sum_{i=1}^{9} N_{i,\xi}(\xi, \eta)\begin{Bmatrix} x_i \\ y_i \\ z_i \end{Bmatrix}^{(j)} + \frac{t_j\zeta^{(j)}}{2}\sum_{i=1}^{9} N_{i,\xi}(\xi, \eta)\boldsymbol{e}_{3i}^{(j)}$$

$$j = 1, 2, 3 \tag{32}$$

$$\frac{\partial}{\partial\eta}\begin{Bmatrix} x \\ y \\ z \end{Bmatrix}^{(j)} = \sum_{i=1}^{9} N_{i,\eta}(\xi, \eta)\begin{Bmatrix} x_i \\ y_i \\ z_i \end{Bmatrix}^{(j)} + \frac{t_j\zeta^{(j)}}{2}\sum_{i=1}^{9} N_{i,\eta}(\xi, \eta)\boldsymbol{e}_{3i}^{(j)}$$

$$j = 1, 2, 3 \tag{33}$$

$$\frac{\partial}{\partial\zeta^{(j)}}\begin{Bmatrix} x \\ y \\ z \end{Bmatrix}^{(j)} = \frac{t_j}{2}\sum_{i=1}^{9} N_i(\xi, \eta)\boldsymbol{e}_{3i}^{(j)}, \qquad j = 1, 2, 3 \tag{34}$$

Note that all three layers have different Jacobian matrices.

F. Strain–Displacement Matrix

For each layer, the strain field is determined from derivatives of displacements in the global coordinates

$$\epsilon = \boldsymbol{H}\boldsymbol{u}_{,k} \tag{35}$$

or, explicitly,

$$\begin{Bmatrix} \epsilon_{xx} \\ \epsilon_{yy} \\ \epsilon_{zz} \\ \epsilon_{xy} \\ \epsilon_{yz} \\ \epsilon_{zx} \end{Bmatrix} = \begin{bmatrix} 1 & 0 & 0 & 0 & 0 & 0 & 0 & 0 & 0 \\ 0 & 0 & 0 & 0 & 1 & 0 & 0 & 0 & 0 \\ 0 & 0 & 0 & 0 & 0 & 0 & 0 & 0 & 1 \\ 0 & 1 & 0 & 1 & 0 & 0 & 0 & 0 & 0 \\ 0 & 0 & 0 & 0 & 0 & 1 & 0 & 1 & 0 \\ 0 & 0 & 1 & 0 & 0 & 0 & 1 & 0 & 0 \end{bmatrix}\begin{Bmatrix} u_{,x} \\ u_{,y} \\ u_{,z} \\ v_{,x} \\ v_{,y} \\ v_{,z} \\ w_{,x} \\ w_{,y} \\ w_{,z} \end{Bmatrix} \tag{36}$$

In addition,

$$\begin{Bmatrix} u_{,x} \\ u_{,y} \\ u_{,z} \\ v_{,x} \\ v_{,y} \\ v_{,z} \\ w_{,x} \\ w_{,y} \\ w_{,z} \end{Bmatrix} = \begin{bmatrix} \Gamma & 0 & 0 \\ 0 & \Gamma & 0 \\ 0 & 0 & \Gamma \end{bmatrix}\begin{Bmatrix} u_{,\xi} \\ u_{,\eta} \\ u_{,\zeta} \\ v_{,\xi} \\ v_{,\eta} \\ v_{,\zeta} \\ w_{,\xi} \\ w_{,\eta} \\ w_{,\zeta} \end{Bmatrix} \tag{37}$$

where

$$\Gamma \equiv \boldsymbol{J}^{-1} = \begin{bmatrix} x_{,\xi} & y_{,\xi} & z_{,\xi} \\ x_{,\eta} & y_{,\eta} & z_{,\eta} \\ x_{,\zeta} & y_{,\zeta} & z_{,\zeta} \end{bmatrix}^{-1} \tag{38}$$

For layers 1 and 3, substitution of Eq. (18) into Eqs. (36) and (37) results in

$$\begin{Bmatrix} \epsilon_{xx} \\ \epsilon_{yy} \\ \epsilon_{zz} \\ \epsilon_{xy} \\ \epsilon_{yz} \\ \epsilon_{zx} \end{Bmatrix}^{(j)} = \sum_{i=1}^{9} \boldsymbol{B}_i^{(j)}\begin{Bmatrix} u_i \\ v_i \\ w_i \\ \alpha_i \\ \beta_i \end{Bmatrix}^{(j)}, \qquad j = 1, 3 \tag{39}$$

where

$$\boldsymbol{B}_i^{(j)} = \boldsymbol{H}\begin{bmatrix} \Gamma^{(j)} & 0 & 0 \\ 0 & \Gamma^{(j)} & 0 \\ 0 & 0 & \Gamma^{(j)} \end{bmatrix} \times \begin{bmatrix} \begin{bmatrix} N_{i,\xi} & 0 & 0 \\ N_{i,\eta} & 0 & 0 \\ 0 & 0 & 0 \end{bmatrix}, \frac{t_j}{2}\begin{bmatrix} \zeta^{(j)}N_{i,\xi} & 0 & 0 \\ \zeta^{(j)}N_{i,\eta} & 0 & 0 \\ N_i & 0 & 0 \end{bmatrix}\Theta_i^{(j)} \\ \begin{bmatrix} 0 & N_{i,\xi} & 0 \\ 0 & N_{i,\eta} & 0 \\ 0 & 0 & 0 \end{bmatrix}, \frac{t_j}{2}\begin{bmatrix} 0 & \zeta^{(j)}N_{i,\xi} & 0 \\ 0 & \zeta^{(j)}N_{i,\eta} & 0 \\ 0 & N_i & 0 \end{bmatrix}\Theta_i^{(j)} \\ \begin{bmatrix} 0 & 0 & N_{i,\xi} \\ 0 & 0 & N_{i,\eta} \\ 0 & 0 & 0 \end{bmatrix}, \frac{t_j}{2}\begin{bmatrix} 0 & 0 & \zeta^{(j)}N_{i,\xi} \\ 0 & 0 & \zeta^{(j)}N_{i,\eta} \\ 0 & 0 & N_i \end{bmatrix}\Theta_i^{(j)} \end{bmatrix}$$

$$j = 1, 3 \tag{40}$$

For layer 2, substitution of Eq. (22) into Eqs. (36) and (37) results in

$$\begin{Bmatrix} \epsilon_{xx} \\ \epsilon_{yy} \\ \epsilon_{zz} \\ \epsilon_{xy} \\ \epsilon_{yz} \\ \epsilon_{zx} \end{Bmatrix}^{(2)} = \sum_{i=1}^{9} \boldsymbol{B}_{i1}^{(2)} \begin{Bmatrix} u_i \\ v_i \\ w_i \\ \alpha_i \\ \beta_i \end{Bmatrix}^{(1)} + \sum_{i=1}^{9} \boldsymbol{B}_{i3}^{(2)} \begin{Bmatrix} u_i \\ v_i \\ w_i \\ \alpha_i \\ \beta_i \end{Bmatrix}^{(3)} \tag{41}$$

where

$$\boldsymbol{B}_{i1}^{(2)} = \boldsymbol{H} \begin{bmatrix} \Gamma^{(2)}\boldsymbol{b}_{1i} & \boldsymbol{0} & \boldsymbol{0} \\ \boldsymbol{0} & \Gamma^{(2)}\mathbf{b}_{1i} & \boldsymbol{0} \\ \boldsymbol{0} & \boldsymbol{0} & \Gamma^{(2)}\boldsymbol{b}_{1i} \end{bmatrix} \left[\boldsymbol{I}, -\frac{t_1}{2}\Theta_i^{(1)} \right] \tag{42}$$

$$\boldsymbol{B}_{i3}^{(2)} = \boldsymbol{H} \begin{bmatrix} \Gamma^{(2)}\mathbf{b}_{3i} & \boldsymbol{0} & \boldsymbol{0} \\ \boldsymbol{0} & \Gamma^{(2)}\mathbf{b}_{3i} & \boldsymbol{0} \\ \boldsymbol{0} & \boldsymbol{0} & \Gamma^{(2)}\mathbf{b}_{3i} \end{bmatrix} \left[\boldsymbol{I}, \frac{t_3}{2}\Theta_i^{(3)} \right] \tag{43}$$

In Eqs. (32) and (43), $\boldsymbol{I}$ is a 3×3 identity matrix, $\boldsymbol{0}$ is a 3×1 zero matrix,

$$\boldsymbol{b}_{1i} = \begin{Bmatrix} \left(1 + \zeta^{(2)}\right) N_{i,\xi}/2 \\ \left(1 + \zeta^{(2)}\right) N_{i,\eta}/2 \\ N_i/2 \end{Bmatrix} \tag{44}$$

$$\boldsymbol{b}_{3i} = \begin{Bmatrix} \left(1 - \zeta^{(2)}\right) N_{i,\xi}/2 \\ \left(1 - \zeta^{(2)}\right) N_{i,\eta}/2 \\ -N_i/2 \end{Bmatrix} \tag{45}$$

Similar to the displacement field, the strain field can be rewritten in a compact form within an element [cf. Eqs. (26–29)] through

$$\begin{Bmatrix} \epsilon_{xx} \\ \epsilon_{yy} \\ \epsilon_{zz} \\ \epsilon_{xy} \\ \epsilon_{yz} \\ \epsilon_{zx} \end{Bmatrix}^{(j)} = \boldsymbol{B}^{(j)}\boldsymbol{d}, \qquad j = 1, 2, 3 \tag{46}$$

For layers 1 and 3, comparison of Eq. (39) with Eq.(46) results in

$$\boldsymbol{B}^{(1)} = \left[\boldsymbol{B}_1^{(1)}, \boldsymbol{B}_2^{(1)}, \ldots, \boldsymbol{B}_9^{(1)}, \boldsymbol{0}, \boldsymbol{0}, \ldots, \boldsymbol{0} \right] \tag{47}$$

$$\boldsymbol{B}^{(3)} = \left[\boldsymbol{0}, \boldsymbol{0}, \ldots, \boldsymbol{0}, \boldsymbol{B}_1^{(3)}, \boldsymbol{B}_2^{(3)}, \ldots, \boldsymbol{B}_9^{(3)} \right] \tag{48}$$

For layer 2, comparison of Eqs. (41) and (46) results in

$$\boldsymbol{B}^{(2)} = \left[\boldsymbol{B}_{11}^{(2)}, \boldsymbol{B}_{21}^{(2)}, \ldots, \boldsymbol{B}_{91}^{(2)}, \boldsymbol{B}_{13}^{(2)}, \boldsymbol{B}_{23}^{(2)}, \ldots, \boldsymbol{B}_{93}^{(2)} \right] \tag{49}$$

G. Stress–Strain Relation

For simplicity, let us drop the superscript (j) tentatively in this section. For layers 1 and 3, the stress–strain relation follows the generalized Hooke's law in the local coordinates. For piezoelectric materials, the generailized Hooke's law is (see Ref. 22)

$$\begin{Bmatrix} \sigma'_{xx} \\ \sigma'_{yy} \\ \sigma'_{xy} \\ \sigma'_{xz} \\ \sigma'_{yz} \\ \sigma'_{zz} \end{Bmatrix} = \begin{bmatrix} C_{11} & C_{12} & 0 & 0 & 0 & C_{13} \\ C_{12} & C_{11} & 0 & 0 & 0 & C_{13} \\ 0 & 0 & (C_{11} - C_{12})/2 & 0 & 0 & 0 \\ 0 & 0 & 0 & C_{44} & 0 & 0 \\ 0 & 0 & 0 & 0 & C_{44} & 0 \\ C_{13} & C_{13} & 0 & 0 & 0 & C_{33} \end{bmatrix} \begin{Bmatrix} \epsilon'_{xx} \\ \epsilon'_{yy} \\ \epsilon'_{xy} \\ \epsilon'_{xz} \\ \epsilon'_{yz} \\ \epsilon'_{zz} \end{Bmatrix} - \begin{Bmatrix} e_{31}E'_z \\ e_{31}E'_z \\ 0 \\ e_{15}E'_x \\ e_{15}E'_y \\ e_{33}E'_z \end{Bmatrix} \tag{50}$$

where C_{ij} are elastic constants, e_{ij} are piezoelectric constants, and E'_x, E'_y, and E'_z are the electric fields along the local coordinates. For degenerate shell theories, the stress state is plane-stress resulting in

$$\sigma'_{zz} = C_{13}(\epsilon'_{xx} + \epsilon'_{yy}) + C_{33}\epsilon'_{zz} - e_{33}E'_z = 0 \tag{51}$$

or

$$\epsilon'_{zz} = (1/C_{33})[e_{33}E'_z - C_{13}(\epsilon'_{xx} + \epsilon'_{yy})] \tag{52}$$

Substitution of Eq. (52) back to Eq. (50) results in

$$\begin{Bmatrix} \sigma'_{xx} \\ \sigma'_{yy} \\ \sigma'_{zz} \\ \sigma'_{xy} \\ \sigma'_{yz} \\ \sigma'_{zx} \end{Bmatrix} = \begin{bmatrix} E_{11} & E_{12} & 0 & 0 & 0 & 0 \\ E_{12} & E_{11} & 0 & 0 & 0 & 0 \\ 0 & 0 & 0 & 0 & 0 & 0 \\ 0 & 0 & 0 & G_{12} & 0 & 0 \\ 0 & 0 & 0 & 0 & G_{23}/\kappa & 0 \\ 0 & 0 & 0 & 0 & 0 & G_{23}/\kappa \end{bmatrix} \begin{Bmatrix} \epsilon'_{xx} \\ \epsilon'_{yy} \\ \epsilon'_{zz} \\ \epsilon'_{xy} \\ \epsilon'_{yz} \\ \epsilon'_{zx} \end{Bmatrix} - \begin{Bmatrix} \mu_{31}E'_z \\ \mu_{31}E'_z \\ 0 \\ 0 \\ e_{15}E'_y \\ e_{15}E'_x \end{Bmatrix} \tag{53}$$

where $E_{11} = C_{11} - C_{13}^2/C_{33}$, $E_{12} = C_{12} - C_{13}^2/C_{33}$, $G_{12} = (C_{11} - C_{12})/2$, $G_{23} = C_{44}$, and $\mu_{31} = e_{31} - C_{13}e_{33}/C_{33}$. In addition, $\kappa = 1.2$ is usually introduced in Eq. (53) to compensate for the shear deformation of the layer. In general, the local stress–strain relation (53) can be written as

$$\sigma' = \boldsymbol{E}'\epsilon' - \sigma'_0 \tag{54}$$

in the local coordinate or

$$\sigma = \boldsymbol{E}\epsilon - \sigma_0 \tag{55}$$

in the global coordinate, where

$$\epsilon' = \Omega_\epsilon \epsilon, \qquad \sigma = \Omega_\epsilon^T \sigma', \qquad \boldsymbol{E} = \Omega_\epsilon^T \boldsymbol{E}' \Omega, \qquad \sigma_0 = \Omega_\epsilon^T \sigma'_0 \tag{56}$$

with Ω_ϵ being the 6×6 transformation matrix consisting of $\boldsymbol{e}_1$, $\boldsymbol{e}_2$, and $\boldsymbol{e}_3$ as shown in Eq. (9).

Theoretically, the constitutive equation (53) is not complete for piezoelectric materials. There is a second set of constitutive equations relating the electric fields E'_x, E'_y, and E'_z and the mechanical strains ϵ' to electric displacements.[22] In other words, the electric field and the mechanical strains are coupled. In many smart structures and

smart materials applications, however, the piezoelectric layers are very thin. In addition, the frequency of interest is low, for example, well below megahertz or microwave range. Therefore, the electric field can be approximated as constant in z' and uniform throughout the layer with good accuracy. Under this approximation, the electric field is independent of the strain field and serves as an external excitation. This condition will be assumed for the rest of the paper.

For layer 2, the stress–strain relation of viscoelastic materials can be described either through complex moduli or relaxation functions. When the system is under sinuoidal excitations of frequency ω, the stress and strain take the complex representations $\sigma_0' e^{j\omega t}$ and $\epsilon_0' e^{j\omega t}$, respectively. Then the stress–strain relation is

$$\sigma_0' = \boldsymbol{E}'(\omega)\epsilon_0' \tag{57}$$

where $\boldsymbol{E}'(\omega)$ is a matrix of complex moduli. If the Poisson's ratio ν is constant and the viscoelastic material is isotropic, $\boldsymbol{E}'(\omega)$ becomes

$$\boldsymbol{E}' = \begin{bmatrix} E(\omega)/(1-\nu^2) & E(\omega)\nu/(1-\nu^2) & 0 & 0 & 0 & 0 \\ E(\omega)\nu/(1-\nu^2) & E(\omega)/(1-\nu^2) & 0 & 0 & 0 & 0 \\ 0 & 0 & 0 & 0 & 0 & 0 \\ 0 & 0 & 0 & G(\omega) & 0 & 0 \\ 0 & 0 & 0 & 0 & G(\omega)/\kappa & 0 \\ 0 & 0 & 0 & 0 & 0 & G(\omega)/\kappa \end{bmatrix} \tag{58}$$

where $G(\omega)$ is the complex modulus in shear and $E(\omega) = 2(1+\nu)G(\omega)$.

If the excitations are not sinusoidal, the stress–strain relation must be represented in terms of a relaxation matrix and a convolution integral as

$$\sigma'(t) = \boldsymbol{R}'(t) \circ \epsilon'(t) \equiv \int_0^t \boldsymbol{R}'(t-\tau)\epsilon'(\tau)\,\mathrm{d}\tau \tag{59}$$

where $\boldsymbol{R}(t)$ is the relaxation matrix and $\circ$ represents the convolution integral.

H. Principle of Virtual Work

Finally, the principle of virtual work is used to derive the equation of motion. Let $\delta\boldsymbol{u}$ be a virtual displacement and $\delta\epsilon$ be the corresponding virtual strain field. In addition, let $\boldsymbol{b}$ and $\boldsymbol{T}$ be the body forces and surface tractions. The principle virtual work states that

$$-\int_V \rho\delta\boldsymbol{u}^T\ddot{\boldsymbol{u}}\,\mathrm{d}V + \int_V \delta\boldsymbol{u}^T\boldsymbol{b}\,\mathrm{d}V + \int_S \delta\boldsymbol{u}^T\boldsymbol{T}\,\mathrm{d}S = \int_V \delta\epsilon^T\sigma\,\mathrm{d}V \tag{60}$$

where ρ is the density and

$$\int_V \mathrm{d}V$$

is the volume integral over all three layers defined as

$$\int_V \mathrm{d}V = \int_V^{(1)} \mathrm{d}V^{(1)} + \int_V^{(2)} \mathrm{d}V^{(2)} + \int_V^{(3)} \mathrm{d}V^{(3)} \tag{61}$$

Note that the differential volumes in Eq. (61) can be represented in terms of the natural coordinates ξ, η, and ζ through Eq. (31). Also in Eq. (60),

$$\int_S \mathrm{d}S$$

is the surface integral on all external surfaces of the structure.

To demonstrate the inertia and stiffness matrices, consider a single element first. Substitution of Eqs. (26), (46), (54), (56), and (59) into Eq. (60) results in

$$\delta\boldsymbol{u}^T\left\{\boldsymbol{M}\ddot{\boldsymbol{d}} + \left[\boldsymbol{K}^{(1)} + \boldsymbol{K}^{(3)}\right]\boldsymbol{d} + \boldsymbol{R}^{(2)} \circ \boldsymbol{d} - \boldsymbol{f}\right\} = \boldsymbol{0} \tag{62}$$

In Eq. (62), $\boldsymbol{M}$ is the mass matrix defined as

$$\boldsymbol{M} = \sum_{j=1}^{3} \int_{-1}^{1}\int_{-1}^{1}\int_{-1}^{1} \rho_j \left[\boldsymbol{N}^{(j)}\right]^T \boldsymbol{N}^{(j)} J^{(j)}\,\mathrm{d}\xi\,\mathrm{d}\eta\,\mathrm{d}\zeta^{(j)} \tag{63}$$

$\boldsymbol{K}^{(1)}$ and $\boldsymbol{K}^{(3)}$ are stiffness matrices defined as

$$\boldsymbol{K}^{(j)} = \int_{-1}^{1}\int_{-1}^{1}\int_{-1}^{1} \left[\boldsymbol{B}^{(j)}\right]^T \Omega_\epsilon^T \left[\boldsymbol{E}^{(j)}\right]' \Omega_\epsilon \boldsymbol{B}^{(j)} J^{(j)}\,\mathrm{d}\xi\,\mathrm{d}\eta\,\mathrm{d}\zeta^{(j)} \qquad j = 1, 3 \tag{64}$$

$\boldsymbol{R}^{(2)}$ is a relaxation matrix defined as

$$\boldsymbol{R}^{(2)} = \int_{-1}^{1}\int_{-1}^{1}\int_{-1}^{1} \left[\boldsymbol{B}^{(2)}\right]^T \Omega_\epsilon^T \boldsymbol{R}' \Omega_\epsilon \boldsymbol{B}^{(2)} J^{(2)}\,\mathrm{d}\xi\,\mathrm{d}\eta\,\mathrm{d}\zeta^{(2)} \tag{65}$$

and $\boldsymbol{f}$ is nodal force vector defined as

$$\boldsymbol{f} = \int_V \boldsymbol{N}^T\boldsymbol{b}\,\mathrm{d}V + \int_S \boldsymbol{N}^T\boldsymbol{t}\,\mathrm{d}S + \boldsymbol{p} + \sum_{j=1,3}\int_{-1}^{1}\int_{-1}^{1}\int_{-1}^{1} \left[\boldsymbol{B}^{(j)}\right]^T \Omega_\epsilon^T \left\{\sigma_0^{(j)}\right\}' J^{(j)}\,\mathrm{d}\xi\,\mathrm{d}\eta\,\mathrm{d}\zeta^{(j)} \tag{66}$$

where $\boldsymbol{t}$ is the distributed component of the surface traction and $\boldsymbol{p}$ is the concentrated load component of the surface traction. Note that the electric field in $\sigma_0^{(j)}$ is assumed to be constant and decoupled from the strain field. Therefore, $\sigma_0^{(j)}$ does not depend on $\delta\boldsymbol{u}$, and the principle of virtual work applies.

When more than one element is present, the nodal displacement vector $\boldsymbol{d}$ needs to be augmented to include the nodal displacements of all elements. Similarly, the mass matrix, stiffness matrix, relaxation matrix, and nodal load vector $\boldsymbol{f}$ all need to be augmented. Finally, boundary conditions are imposed, and $\delta\boldsymbol{u}$ needs to remain arbitrary. This will result in an equation of motion that often takes the form

$$\boldsymbol{M}\ddot{\boldsymbol{d}} + \left[\boldsymbol{K}^{(1)} + \boldsymbol{K}^{(3)}\right]\boldsymbol{d} + \boldsymbol{R}^{(2)} \circ \boldsymbol{d} = \boldsymbol{f} \tag{67}$$

where all of the quantities are in the augmented form. When the system is subjected to sinusoidal excitations $\boldsymbol{f} = \boldsymbol{f}_0 e^{j\omega t}$ and undergoes sinusoidal response $\boldsymbol{d} = \boldsymbol{d}_0 e^{j\omega t}$, equation of motion (67) can be rewritten as

$$\left[\boldsymbol{K}^{(1)} + \boldsymbol{K}^{(2)}(\omega) + \boldsymbol{K}^{(3)} - \omega^2\boldsymbol{M}\right]\boldsymbol{d}_0 = \boldsymbol{f}_0 \tag{68}$$

where

$$\boldsymbol{K}^{(2)}(\omega) = j\omega\mathcal{F}\left\{\boldsymbol{R}^{(2)}\right\} = \int_{-1}^{1}\int_{-1}^{1}\int_{-1}^{1} \left[\boldsymbol{B}^{(2)}\right]^T \Omega_\epsilon^T \left\{\boldsymbol{E}^{(2)}(\omega)\right\}' \times \Omega_\epsilon \boldsymbol{B}^{(2)} J^{(2)}\,\mathrm{d}\xi\,\mathrm{d}\eta\,\mathrm{d}\zeta^{(2)} \tag{69}$$

In Eq. (69), $\mathcal{F}\{\cdot\}$ is the Fourier transform and $\{\boldsymbol{E}^{(2)}(\omega)\}'$ is the matrix of complex moduli given in Eq. (58).

III. Numerical Examples

A MATHEMATICA-based finite element code, VDPCL, using the described formulation has been developed. MATHEMATICA is chosen as the language of VDPCL because it is easy to program, is interactive, and has a powerful graphic interface. Nevertheless, the program takes longer execution time and more memory.

Verification of the program and the formulation consists of four parts: patch tests, eigenvalue analysis, forced response, and locking. Plate elements were used in the first three parts, and shell elements were used in the last part. They are explained in detail as follows.

A. Patch Tests

Numerous static and dynamic patch tests were performed to check the convergence and validity of the formulations. In these tests, the structure is a rectangular plate, and all three layers consist of the same elastic material. Therefore, the numerical results should converge to those of isotropic rectangular plates, which are available in many textbooks. Various tests have been performed for simply supported and clamped boundary conditions, as well as different numbers of elements. For static tests, deflections of the plate subjected to a concentrated load from analytical and numerical calculations are compared. For dynamic tests, natural frequencies of the plate are compared. The results of the patch tests are satisfactory. The details of the results and the tests may be found in Ref. 23.

B. Eigenvalue Analysis

The purpose of this test is to calculate eigenvalues, that is, natural frequencies and loss factors, of a damped rectangular sandwich plate

Table 1 Eigenvalues obtained by VDPCL, NASTRAN, and analytical solutions

	Natural frequency, Hz			Loss factor		
Mode	Analytical solution	NASTRAN (10 × 12)	VDPCL (5 × 6)	Analytical solution	NASTRAN (10 × 12)	VDPCL (5 × 6)
1	60.3	57.4	56.9	0.190	0.176	0.180
2	115.4	113.2	111.9	0.203	0.188	0.190
3	130.6	129.3	127.5	0.199	0.188	0.187
4	178.7	179.3	174.9	0.181	0.153	0.164
5	195.7	196.0	193.1	0.174	0.153	0.158

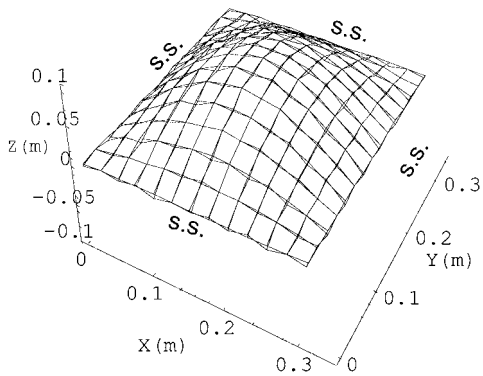

a) $\omega_1 = 56.96$ Hz

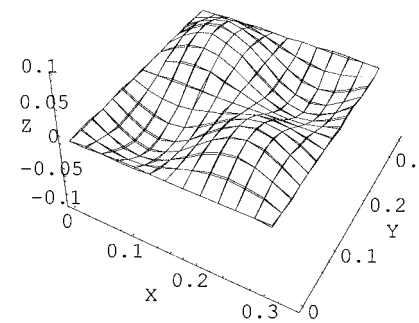

d) $\omega_4 = 174.49$ Hz

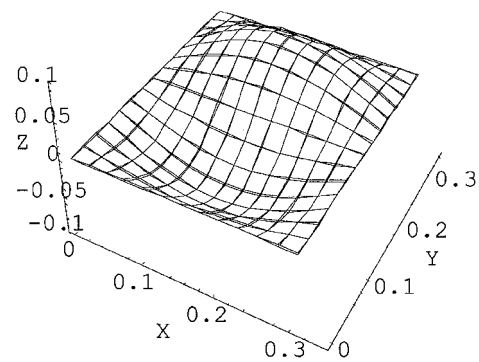

b) $\omega_2 = 111.81$ Hz

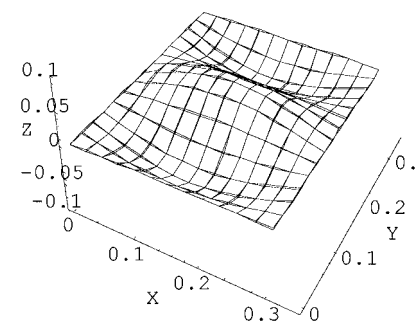

e) $\omega_5 = 192.18$ Hz

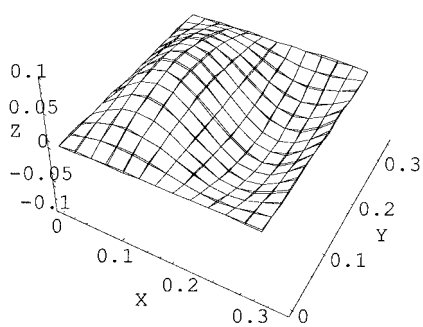

c) $\omega_3 = 127.35$ Hz

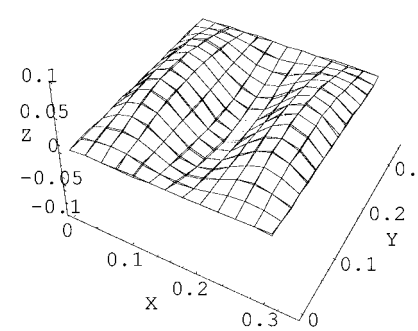

f) $\omega_6 = 230.58$ Hz

Fig. 5 First six mode shapes obtained from VDPCL.

through use of complex moduli. The numerical results are compared with those from NASTRAN and analytical solutions.

Johnson and Kienholz[5] analyzed rectangular sandwich plate with simply supported boundary conditions using a NASTRAN model with 10×12 elements. They compared the NASTRAN results with the existing closed-form solution when the damped plate is simply supported. The NASTRAN results were based on the modal strain energy method with constant values of viscoelastic shear modulus and loss factor.

Dimensions and material properties of the damped sandwich plate are as follows. A 30.48×34.80 cm (12.0×13.69 in.) rectangular sandwich plate is analyzed with 2×2, 3×3, 4×4, 5×6, and 6×7 elements. The thickness of the upper and lower layers are both 0.762 mm (0.030 in.), and the layers have the material properties $E_1 = E_3 = 6.89 \times 10^4$ MPa (1×10^7 psi), $\nu = 0.30$, and $\rho_1 = \rho_3 = 2.74$ g/cm^3 (0.0988 lb/in.^{3}). The viscoelastic layer is 0.254 mm (0.010 in.) thick, and its material properties are $G_2 = 0.896$ MPa (130 psi), $\nu = 0.49$, $\rho_2 = 0.999$ g/cm^3 (0.0361 lb/in.^{3}), and $\eta_2 = 0.50$.

Based on the preceding geometric data and material properties, Table 1 compares eigenvalues (natural frequencies and loss factors) for the first five modes obtained from the analytical solution, NASTRAN, and VDPCL. The NASTRAN simulation uses 10×12 elements, whereas the VDPCL uses 5×6 elements. Table 1 shows that the VDPCL can achieve the same degree of accuracy as NASTRAN with substantially fewer elements (30 vs 120). In addition, Fig. 5 shows the mode shapes obtained from VDPCL with 6×7 elements. Numerous convergence tests have been conducted for the eigenvalue analysis. The details of the test results may be found in Ref. 23.

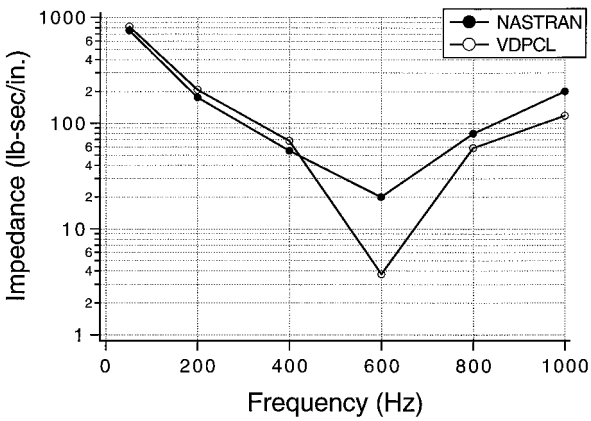

Fig. 6 Mechanical impedance obtained by VDPCL and NASTRAN.

C. Forced Response

The purpose of this test is to calculate forced response of a rectangular damped plate and compare the results with those in the existing literature. Lu et al.[24] analyzed the mechanical impedance, that is driving force divided by velocity, of a damped plate by using NASTRAN and compared the impedance with analytical results obtained by Rao and Nakra.[25]

The dimensions and material properties of the damped sandwich plate are as follows. An acrylic base viscoelastic material (3M SJ2015X) is sandwiched between a steel base plate and a steel constraining layer. The thicknesses of the base plate, viscoelastic layer, and the constraining layer are 12.7 (0.5), 0.1524 (0.006), and 3.175 mm (0.125 in.), respectively. The dimensions of the plate are 0.3556×0.3556 m (14×14 in.). The plate is simply supported, and the driving point is the center of the damped plate. In addition, the driving frequencies are 50, 200, 400, 600, 800, and 1000 Hz. Table 2 and Fig. 6 show the comparison of the mechanical

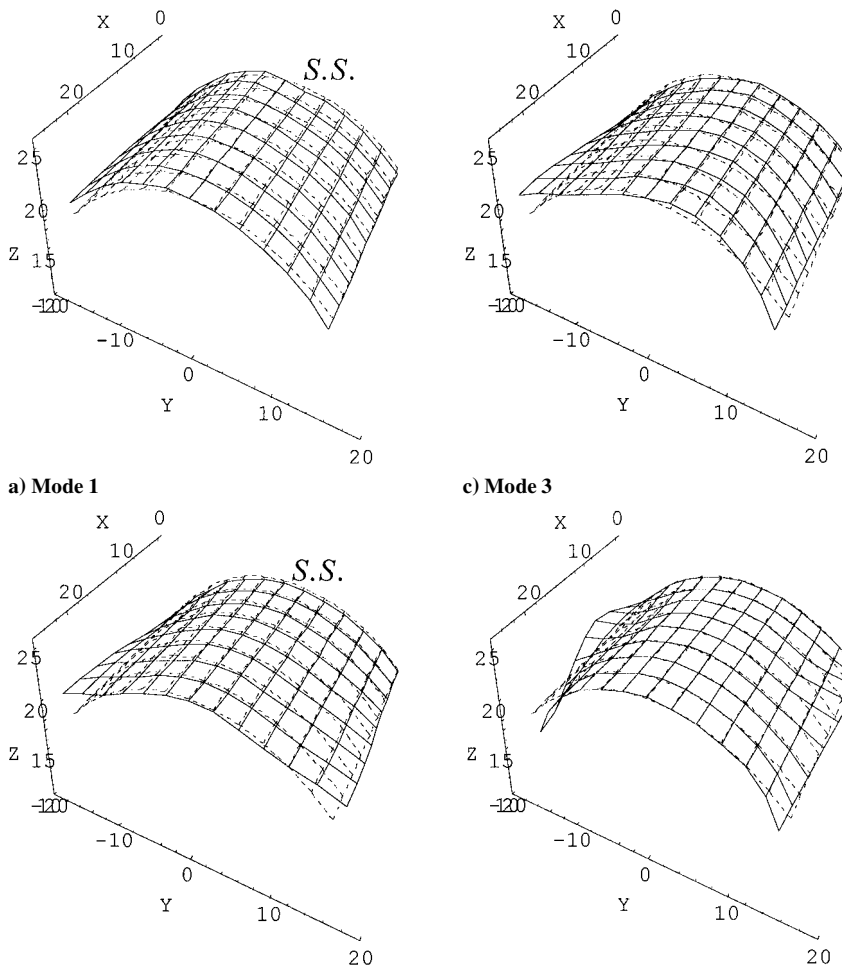

Fig. 7 Spurious mode control in dynamic analysis of a cylindrical roof.

Table 2 Mechanical impedance obtained by VDPCL and NASTRAN

Driving frequency, Hz	NASTRAN, lb · s/in.	VDPCL, lb · s/in.
50	750	819.74
200	175	207.09
400	55	67.94
600	20	3.72
800	80	58.53
1000	200	118.07

impedance obtained from NASTRAN[2,24] and VDPCL. The results from NASTRAN and VDPCL agree reasonably well. Note that the impedance at 600 Hz is small indicating the presence of a resonance. In fact, an eigenvalue analysis of the damped plate shows that the first natural frequency is 596 Hz.

D. Locking

When the three-dimensional degenerate shell elements were introduced,[19] the order of numerical integration was 3×3 for all energy terms including membrane, shear, and bending energies. This is known as full integration, and the results are reasonable for thick shells.

When the shell gets thinner, the full integration imposes too many constraints. As a result, the numerical results become too stiff and show a very slow convergence rate. This phenomenon is call locking (either membrane or shear). To alleviate locking, reduced integration points (2×2) are proposed,[26] which is known as reduced integration. The reduced integration, however, could make stiffness matrix rank deficient resulting in spurious modes (or zero energy modes), which undergo large displacements without any change in strain energy in the absence of proper displacement boundary conditions. Since then, a great deal of research effort has been devoted to eliminating the spurious modes. Major approaches include combination of the shape functions of eight-node and nine-node elements, e.g., heterosis element[27]; nine-node assumed natural strain element by Park and Stanley[28]; and projection methods by introducing additional stabilization matrices into the element stiffness matrix, for example, the γ projector method.[29]

Figure 7 shows dynamic response of a cylindrical roof with spurious mode control using the projetion method. Implementation of the spurious mode control to constrained layer shell elements requires major efforts and perhaps novel approaches. Therefore, it is not pursued in the present paper.

IV. Conclusions

1) An 18-node degenerate constrained layer element is developed for plate and shell structures.

2) For thin plate structures, numerical results show that the isoparametric element can predict natural frequencies, loss factors, and mechanical impedances that are as accurate as NASTRAN with substantially fewer elements.

3) For thin shell structures, applications of the isoparametric formulation are possible, if spurious modes control can be implemented.

Acknowledgments

The first author thanks Daewoo Heavy Industries for a fellowship to support this research. The second author extends thanks to the Army Research Office for supporting the research under Grant DAAG55-98-1-0387.

References

[1]Nashif, A. D., Jones, D. I. G., and Henderson, J. P., *Vibration Damping*, Wiley, New York, 1995, Chap. 6.

[2]Sun, C. T., and Lu, Y. P., *Vibration Damping of Structural Elements*, Prentice–Hall, New York, 1995, Chaps. 4–7.

[3]Lu, Y. P., Killian, J. W., and Everstine, G. C., "Vibrations of Three Layered Damped Sandwich Plate Composites," *Journal of Sound and Vibration*, Vol. 64, 1979, pp. 63–71.

[4]Soni, M. L., and Bogner, F. K., "Finite Element Vibration Analysis of Damped Structures," *AIAA Journal*, Vol. 20, No. 5, 1982, pp. 700–707.

[5]Johnson, C. D., and Kienholz, D. A., "Finite Element Prediction of Damping in Structures with Constrained Viscoelastic Layers," *AIAA Journal*, Vol. 20, No. 9, 1982, pp. 1284–1290.

[6]Lu, Y. P., and Killian, J. W., "A Finite Element Approximation for Damping Material Used in Constrained Damped Structures," *Journal of Sound and Vibration*, Vol. 97, No. 2, 1984, pp. 352–354.

[7]Imaino, W., and Harrison, J. C., "A Comment on Constrained Layer Damping Structures with Low Viscoelastic Modulus," *Journal of Sound and Vibration*, Vol. 149, No. 2, 1991, pp. 354–359.

[8]Macé, M., "Damping of Beam Vibrations by Means of a Thin Constrained Viscoelastic Layer: Evaluation of a New Theory," *Journal of Sound and Vibration*, Vol. 172, No. 5, 1994, pp. 577–591.

[9]Ioannides, E., and Grootenhuis, P., "A Finite Element Analysis of the Harmonic Response of Damped Three-Layer Plates," *Journal of Sound and Vibration*, Vol. 67, 1979, pp. 203–218.

[10]Rikards, R., Chate, A., and Barkanov, E., "Finite Element Analysis of Damping the Vibrations of Laminated Composites," *Computers and Structures*, Vol. 47, No. 6, 1993, pp. 1005–1015.

[11]Rao, V. S., Sankar, B. V., and Sun, C. T., "Constrained Layer Damping of Initially Stressed Composite Beams Using Finite Elements," *Journal of Composite Materials*, Vol. 26, No. 12, 1992, pp. 1752–1766.

[12]Ramesh, T. C., and Ganesan, N., "Orthotropic Cylindrical Shells with a Viscoelastic Core: a Vibration and Damping Analysis," *Journal of Sound and Vibration*, Vol. 175, 1994, pp. 535–555.

[13]Ramesh, T. C., and Ganesan, N., "Vibration and Damping Analysis of Cylindrical Shells with Constrained Damping Treatment—a Comparion of Three Thoeries," *Journal of Vibration and Acoustics*, Vol. 117, No. 2, 1995, pp. 213–219.

[14]Holman, R. E., and Tanner, J. M., "Finite Element Modeling Techniques for Constrained Layer Damping," *AIAA Journal*, Vol. 21, No. 5, 1983, pp. 792–794.

[15]Ma, B. A., and He, J. F., "A Finite Element Analysis of Viscoelastically Damped Sandwich Plates," *Journal of Sound and Vibration*, Vol. 152, No. 1, 1992, pp. 107–123.

[16]Kosmatka, J. B., and Liguore, S. L., "Review of Methods for Analyzing Constrained-Layer Damped Strctures," *Journal of Aerospace Engineering*, Vol. 6, 1993, pp. 268–283.

[17]Baber, T. T., Maddox, R. A., and Orozco, C. E., "A Finite Element Model for Harmonically Excited Viscoelastic Sandwich Beams," *Computers and Structures*, Vol. 66, No. 1, 1998, pp. 105–113.

[18]Bathe, K. J., and Dvorkin, E. N., "A Formulation of General Shell Elements—the Use of Mixed Interpolation of Tensorial Components," *Internation Journal of Numerical Methods for Engineering*, Vol. 22, No. 3, 1986, pp. 697–722.

[19]Ahmad, S., Iron, B., and Zienkiewicz, O. C., "Analysis of Thick and Thin Shell Structures by Curved Finite Elements," *International Journal of Numerical Methods for Engineering*, Vol. 2, 1970, pp. 419–451.

[20]Cook, R. D., Malkus, D. S., and Plesha, M. E., *Concepts and Applications of Finite Element Analysis*, Wiley, New York, 1988, pp. 163–180.

[21]MacNeal, R. H., and Harder, R. L., "Eight Nodes or Nine?" *International Journal of Numerical Methods for Engineering*, Vol. 33, No. 5, 1992, pp. 1049–1058.

[22]Tiersten, H. F., *Linear Piezoelectric Plate Vibrations*, Plenum, New York, 1969, pp. 33–47.

[23]Jeung, Y. S., "Finite Element Analyses for Sandwich Structures with a Viscoelastic Constrained Layer," Ph.D. Dissertation, Dept. of Aeronautics and Astronautics, Univ. of Washington, Seatle, WA, 1998.

[24]Lu, Y. P., Clemens, J. C., and Roscoe, A. J., "Vibrations of Composite Plate Structures Consisting of Constrained-Layer Damping Sandwich with Viscoelastic Core," *Journal of Sound and Vibration*, Vol. 158, No. 3, 1992, pp. 552–558.

[25]Rao, Y. V. K. S., and Nakra, B. C., "Vibrations of Unsymmetrical Sandwich Beams and Plates with Viscoelastic Cores," *Journal of Sound and Vibration*, Vol. 34, 1974, pp. 309–326.

[26]Zienkiewicz, O. C., Taylor, R. L., and Too, J. M., "Reduced Integration Technique in General Analysis of Plates and Shells," *International Journal of Numerical Methods for Engineering*, Vol. 3, 1971, pp. 275–290.

[27]Hughes, T. J. R., and Cohen, M., "The Heterosis Finite Element for Plate Bending," *Computers and Structures*, Vol. 9, 1978, pp. 445–450.

[28]Park, K. C., and Stanley, G. M., "A Curved C^0 Shell Element Based of Assumed Natural Coordinate Strains," *Journal of Applied Mechanics*, Vol. 53, No. 2, 1986, pp. 278–290.

[29]Belytschko, T., Liu, W. K., Ong, J. S. J., and Lam, D., "Implementation and Application of a 9-node Lagrange Shell Element with Spurious Control," *Computers and Structures*, Vol. 20, 1985, pp. 121–128.

A. M. Baz
Associate Editor